The potential of close-range photogrammetry in evaluating the severity of road surface deformations

Mihnea Cățeanu[1], Sorina Mihaela Miclescu[2]

[1] Dept. of Forest Engineering, Forest Management Planning and Terrestrial Measurements, Faculty of Silviculture and Forest Engineering, Transilvania University of Brașov, Șirul Ludwig van Beethoven 1, 500123 Brașov, Romania – cateanu.mihnea@unitbv.ro

[2] Dept. of Geomorphology, Pedology, Geomatics, Faculty of Geography, Bucharest University, Nicolae Bălcescu Boulevard 1, District 1, 010041 Bucharest, Romania – sorina.mihaela81@gmail.com

Keywords: close-range photogrammetry, Structure-from-Motion, road surface deformations, 3D surface reconstruction, LiDAR.

Abstract

This study evaluates the use of close-range photogrammetry, specifically the Structure-from-Motion (SfM) technique, for assessing road surface deformations. Utilizing a low-cost GoPro Hero 10 action camera, 3D models were created for a 45-meter degraded road section, in order to calculate the volume of road surface defects. Three image collection strategies were compared: only near-nadiral imagery, and near-nadiral plus one or two tracks of oblique images, respectively. Reference data was obtained from Terrestrial Laser Scanning (TLS), in order to assess the level of accuracy for deformation volumes calculated from SfM data. The photogrammetric models, scaled and georeferenced using Ground Control Points (GCPs), allowed for an accurate assessment of deformation volumes (RMSEs of 0.16–0.18 dm^3 for the 32 potholes identified in the studied sector) and road surface reconstruction (with average displacements between SfM and TLS point clouds of 0.007–0.013 meters). Deformation volumes extracted from SfM 3D models of the road surface are highly correlated with reference volumes from TLS data, regardless of image collection strategy. However, using at least one track of oblique image collection leads to an accuracy improvement. Our findings confirm that close-range photogrammetry with a low-cost, easily available action camera, is an effective, cost-effective alternative for monitoring road deformations, offering high-resolution 3D models suitable for precise volume and depth measurements. However, the technique does have some limitations, mainly related to the need of GCPs in order to scale the 3D models and the significant amount of manual labour necessary in order to calculate the volume of road surface defects.

1. Introduction

Road surface deformations, especially if left unmonitored, are a significant concern for the transportation infrastructure (Mroczkowski, 2009; Sun et al., 2023), as they have an impact on safety (Grygierek and Zieba, 2019) and increase vehicle maintenance costs (Zeng et al., 2013). Some of the main causes of road surface damage (potentially leading to the formation of defects such as cracks, potholes or patches) are improperly bound granular materials in the asphalt basecourse (Werkmeister et al., 2015), mechanical loads from vehicle wheels (Pankov, 2022) or climatic factors such as freezing and thawing cycles (Wang et al., 2023). The identification and monitoring of deformations is a pressing issue for maintaining road safety and infrastructure longevity, as delaying maintenance activities can lead to major structural and functional deterioration of the road infrastructure (Peraka and Biligiri, 2020). The ability to detect road surface defects and estimate their severity (in terms of, for e.g., maximum depth, area and/or volume) helps authorities make data-driven decisions for preventive maintenance, ensure road safety and reduce long-term costs (Eker, 2023).

For a long time, the identification of road surface deformations has been done manually by visual surveys, but this approach is problematic due to factors such as low time-efficiency (Kargah-Ostadi et al., 2017) and high costs. Therefore, the exploration of automatic methods for characterizing road surface deformations has been an active area of research. Equipment designed specifically for monitoring road surfaces has been developed in the past (Vilaça et al., 2010), but generally involves high acquisition costs and trained personnel.

On the other hand, road surface deformations can be detected and measured using more general surveying methods, not designed specifically for this purpose. Common approaches include the use of: geodetic surveys carried out with GNSS (Global Navigational Satellite Systems) and total station (Hrůza et al., 2018), Unmanned Aerial Vehicles (UAV) (Jia Yi and Ahmad, 2023; Zhang and Elaksher, 2012), Terrestrial Laser Scanning (TLS) (Akgul et al., 2017; Jia Yi and Ahmad, 2023) or Mobile Laser Scanning (MLS) (De Blasiis et al., 2020; Haiyan Guan et al., 2015), accelerometer data collected by smartphone devices (Dong and Li, 2021) or multi-sensor systems (Chen et al., 2016). These instruments collect 2D and/or 3D data which is afterwards used to detect the presence (and potentially the severity) of defects such as cracks or potholes by manual, semi-automatic or automatic processing.

In the field of photogrammetry, a relatively recent development is that of close-range photogrammetry (also called Structure-from-Motion, or SfM in short). SfM operates on the same methods and principles of digital photogrammetry, but uses image-matching algorithms developed by the computer vision community to solve the problem of image alignment (Nadal-Romero et al., 2015). Because of this, the orientation and distortion of the camera are no longer needed, so close-range photogrammetry can be carried out with inexpensive, non-photogrammetric cameras. This makes it ideally suited for low-cost data acquisition (Westoby et al., 2012). The continuous development of cheap or even freely available software solutions for the processing of SfM-acquired data and the lowering costs of digital cameras capable of acquiring high-resolution imagery have led to a wider adoption of close-range photogrammetry as an alternative to other established data collection methods in

geomatics. As such, SfM has been used to quantify erosion and deposition processes (Nadal-Romero et al., 2015; Peter Heng et al., 2010; Smith and Vericat, 2015), survey heritage sites (Del Pozo et al., 2020; Morena, 2022), map topographical surfaces (Gonçalves et al., 2016; James and Robson, 2012), estimate forest tree diameters (Mokroš et al., 2018) or generate 3D reconstructions of entire forest tree stands (Kuželka and Surový, 2021).

Since images acquired from different camera positions allow for the reconstruction of a high-accuracy 3D model, SfM has been considered as a source for collecting the data necessary to evaluate road surface conditions. For example, close-range photogrammetry has been successfully employed for measuring deformations of forest road surfaces due to timber harvesting (Eker, 2023; Pierzchała et al., 2016, 2014), surveying pavement distress (Ahmed et al., 2011) or automatically identifying cracks (Sarsam, 2019) and rutting (Sarsam et al., 2016) of asphalt road surfaces.

Given the context outlined above, the aim of this study is to establish the potential of close-range photogrammetry for evaluating the volume of road surface deformations, using a low-cost action camera (Hero GoPro 10). To test the feasibility of close-range photogrammetry for this purpose, a study was carried out on a short section of asphalt road that is in very poor condition and has numerous potholes. Light Detection and Ranging (LiDAR) data was collected with a FARO Focus S TLS instrument, to serve as a benchmark for estimating the accuracy of the SfM 3D-reconstructed road surface, both in terms of overall level of agreement and in terms of pothole volume estimations.

2. Methodology

2.1 Study area

A 45-metre sector of public road covered with asphalt was chosen for this study, due to its poor condition and numerous potholes of varying areas and depths. The road sector is located in the "Dumbrăvița" municipality of the "Brașov" county, in the central part of Romania (Figure 1). The road surface is in a highly degraded state, as large quantities of timber have been transported over the last decades because this road connects a network of forest roads to the main artery in the area. A total of 32 potholes were identified visually in the field and subsequently marked with fluorescent spray paint, to aid in their identification on the acquired datasets (Figure 2).

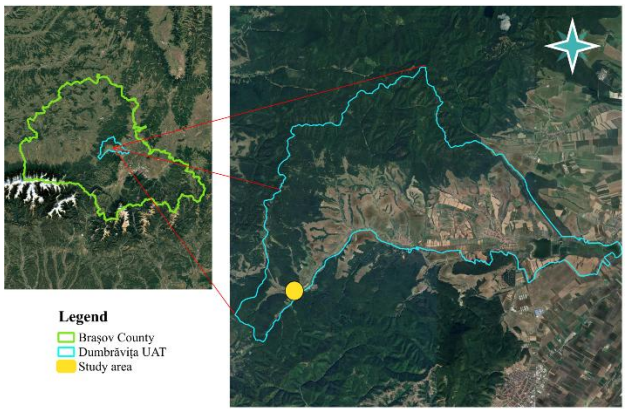

Figure 1. General location of study area

(Background image copyright: ® Airbus 2024, Google Earth).

Figure 2. (a) Defects of varying severity as seen from the ground; (b) defects as seen from aerial imagery collected via UAV (Unmanned Aerial Vehicle) photogrammetry, after marking with fluorescent paint.

2.2 Data collection via close-range photogrammetry

Before images were captured using a GoPro Hero10 action camera, 6 metal bollards were driven into the road surface, to serve as Ground Control Points (GCPs). These bollards were marked with spray paint, to aid in their identification on subsequently collected images (Figure 3a). The coordinates for these points were determined in the *Stereographic 1970* reference system, by topographical survey. This involved using a total station and two reference points established near the study area, determined using Real-Time Kinematic (RTK) GNSS. These GCPs have a dual purpose: (1) they allow for data collected using different sensors to be georeferenced in the same system and (2) they are necessary to properly scale the models, as the GoPro Hero10 instrument is not a photogrammetric camera.

Figure 3. (a) Metal bollards driven into the road surface to serve as GCPs; (b) TLS scanning with checkboard reference targets, which are also installed on the metal bollards.

Images of the road surface were collected from a height of approx. 2 metres, by mounting the GoPro Hero 10 camera on a monopod and carrying it on foot over the study area in four parallel tracks, as follows:

- Two near-nadiral tracks, on either side of the road (Figure 4).
- Two tracks of oblique imagery collected at an angle of approx. 45 degrees, one from each side of the road.
-

Figure 4. Collection of near-nadiral images from a height of approx. 2 meters, using a GoPro Hero 10 action camera mounted on a monopod.

Images were collected automatically using a time lapse of 1-second. The number of images per track varies between 89 and 97, due to the slight changes with which the operator moved across the road section. A total number of 371 images were collected in this manner. The following parameters were used for image collection using the GoPro Hero10 action camera: linear lens setting (i.e. wide FoV but without fisheye effect), focal length 2.71, F-stop F/2.5 and an image resolution of 5568x4176 pixels.

2.3 Reference data collection via TLS (Terrestrial Laser Scanning)

To test the accuracy of close-range photogrammetry for estimating the severity of deformations, reference data was collected using a Faro Focus S LIDAR scanner. Five scanning stations were set up, at distances of 20-25 meters and alternating from one side of the road to the other. Three of the stations were located inside the analysed sector, one before it and the last one after it, respectively. The LiDAR instrument was set to record data at a fraction of 1/2 from full scanning capacity, which corresponds to an average point spacing of 3.1 mm at 10 metres from the scanner and a scan time of 19 minutes. The five scans were aligned and georeferenced in the Faro SCENE software, using the checkerboard targets installed in the field (Figure 3b). Accuracy indicators and the amount of overlap between adjacent scans are presented in Table 1.

Scan no.	Avg. error (mm)	Max. error (mm)	Min. overlap (%)
1	11.5	11.5	54.0
2	7.7	11.5	54.0
3	3.5	3.9	47.6
4	3.0	3.2	47.6
5	5.8	8.8	47.9

Table 1: Accuracy and overlap between individual TLS stations.

2.4 Volume estimation for road surface defects

A methodology was developed to identify each road surface defect (i.e. pothole) and estimate the associated deformation in terms of volume. This involves the following steps:

- Each pothole extent is vectorised, based on visual assessment of the orthomosaic generated from close-range photogrammetry data at a resolution of 0.001 meters, aided by the spray paint markings (Figure 5a).
- A 0.05-metre buffer is applied for each polygon representing a pothole extent; the resulting ring-shaped area represents the road surface area immediately adjacent to a deformation but not yet affected by it - usually called "surrounding non-defect" surface (Koch and Brilakis, 2011).
- Polygons are used for segmentation, obtaining a dataset of points located inside the defect) and each ring-shaped buffer (obtaining a set of points surrounding the defect).
- From each point cloud thus obtained an elevation grid is interpolated at a 0.01-meter resolution; in this manner two elevation models are generated for each defect: a model of the defect itself (Figure 5b) and a model that estimates the road surface it the defect would not have been present (Figure 5c).
- For each defect, the two elevation models are used to estimate the volume of deformation in the *Global Mapper v 25.0* software using the "*Terrain Analysis - Measure Volume between Surfaces*" tool.

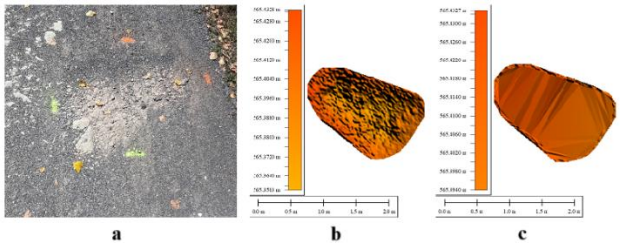

Figure 5. (a) An example of pothole affecting the road surface; (b) 3D model of the area inside the pothole; (c) 3D model of the corresponding road surface, if the defect would not have been present (used to estimate the volume of deformation).

Given the relatively low volumes involved in the analysis, all volume values are reported in cubic decimetres (dm^3), instead of cubic meters.

3. Results

3.1 3D reconstruction of the road surface from close-range photogrammetry data

To evaluate the potential benefit of collecting not only nadiral, but also oblique images of the road surface, 3D surface reconstruction was done in *Agisoft Metashape v. 2.1.1* software using three approaches (Figure 6):

- Two near-nadiral tracks plus two tracks of oblique images (one from each side of the road), totalling 382 images, out of which 379 were aligned by the software (further referred to as *double_oblique*).
- Two near-nadiral tracks plus one track of oblique data collection, totalling 288 images (further referred to as *single_oblique*).
- Two near-nadiral tracks totalling 180 images (further referred to as *nadiral*).

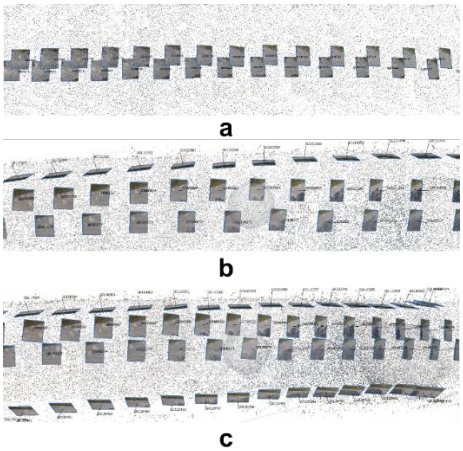

Figure 6. Three strategies for surface reconstruction from close-range imagery: using two near-nadiral tracks (a), adding a single oblique track (b) and adding two oblique tracks (c).

After image alignment, GCPs were used to georeference and scale the models. Afterwards, models were built from the overlapping images, with *Quality* set to "*High*" and *Face count* set to "*Medium*". Finally, point clouds were generated from the models, using the "*High*" setting. The resulting point clouds contain between 66.7 and 86.7 million points and have average densities of 5.5 – 7.1 points/cm^2. As can be seen in Figure 7,

close-range photogrammetric point clouds do not reach the highest densities achievable by LiDAR scanning, but on the other hand have a better spatial distribution. The LiDAR point cloud density exhibits a common pattern, with a very high number of points near the scanning positions and densities falling rapidly as the distance to the scanner increases (Figure 7d).

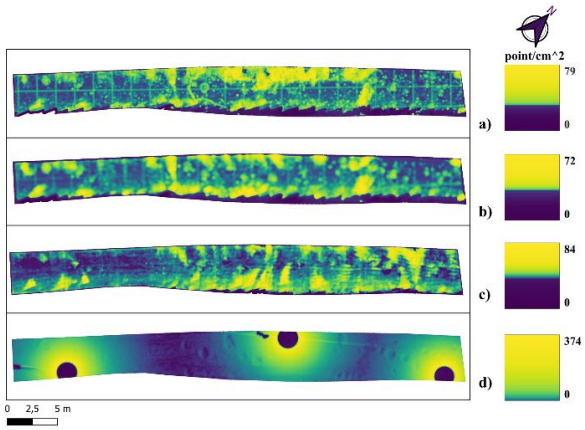

Figure 7. Point cloud density distribution for the *double_oblique* (a), *single_oblique* (b) and *nadiral* (c) variants for 3D surface reconstruction. For comparison, (d) shows the density for the point cloud obtained from LiDAR scanning.

The degree of overlap between point clouds generated from GoPro action camera imagery and the reference dataset was determined using the *M3C2* algorithm (Lague et al., 2013) in *CloudCompare v.2.13.0*, which measures the displacement between two overlapping point clouds (Figure 8). The *double_oblique* and the *single_oblique* point clouds show an average displacement of -0.007 m (std. dev. = 0.02m), while the *nadiral* one has an average displacement of 0.013 m (std. dev. = 0.02m). These results show a very good overall level of agreement between photogrammetric and laser scanning points clouds, with no significant bias in terms of under- or over-estimation of the road surface's height.

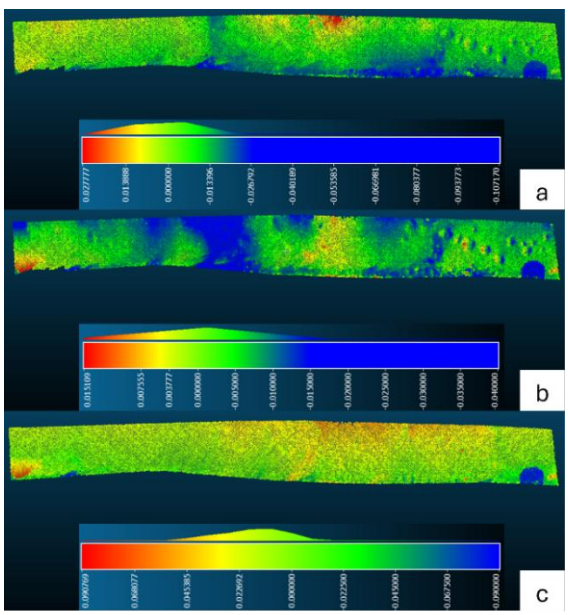

Figure 8. Displacement between the reference point cloud (obtained by LiDAR scanning) and points clouds generated from close-range photogrammetry, using the *double_oblique* (a), *single_oblique* (b) and *nadiral* (c) approaches.

3.2 Estimating the severity of road surface defects

A number of 32 defects affecting the road surface (all classified as potholes) were identified in the field and subsequently on the orthomosaic collected via aerial photogrammetry, with extents ranging from 0.21 to 1.70 m^2 and an average extent of 0.65 m^2 (Figure 9). Deformations were calculated from the TLS point cloud (to serve as reference). The *nadiral* variant, which did not use any oblique imagery, was found to have gaps on the left side of the road section. Because of this, some of the volume deformations could not be calculated from this dataset. Therefore, deformation volumes estimated from close-range photogrammetry data are presented only for the *oblique* and *double_oblique* variants. Deformations range in volume from 1.1 to 33.2 dm^3, with an average of 9.1 dm^3 and a total deformation volume for the studied road section of 290.2 dm^3.

Figure 9. Road surface defects affecting the analysed road section.

More severe defects (having both a larger area and a bigger depth) are easily identifiable on 3D models of the road surface, regardless of how those models are generated (from LiDAR scanning or close-range photogrammetry). For illustration purposes, we present the situation for the most severe deformation of the study area (the largest in terms of both surface and volume). The defect is discernible on DTMs of the road surface, both in top and cross-section views (Figure 10 and Figure 11a, respectively). On the other hand, the small deformations (in terms of surface and depth) are not easily distinguishable on 3D model visualisations. However, they can be identified on cross-section views (Figure 11b), but this is hindered by the fact that the road surface itself has quite a significant inclination.

Since the models generated from images collected using the GoPro action camera have been scaled and georeferenced using GCPs, various characteristics of the defects can be measured directly on the 3D models. These characteristics include affected area, shape, length and width of deformation, maximum depth or volume.

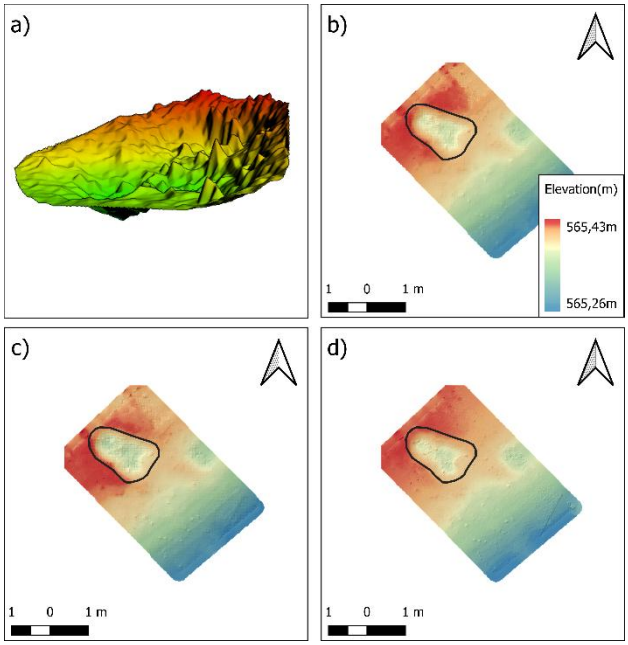

Figure 10. 3D reconstruction of a road surface defect from close-range photogrammetry (a); the same defect as seen on 3D models interpolated at a 0.01 resolution, from close-range imagery collected in the *double_oblique* (b), *single_oblique* (c) and *nadiral* (d) variants. The black line in (b)-(d) represents the extent of the pothole, as marked in the field.

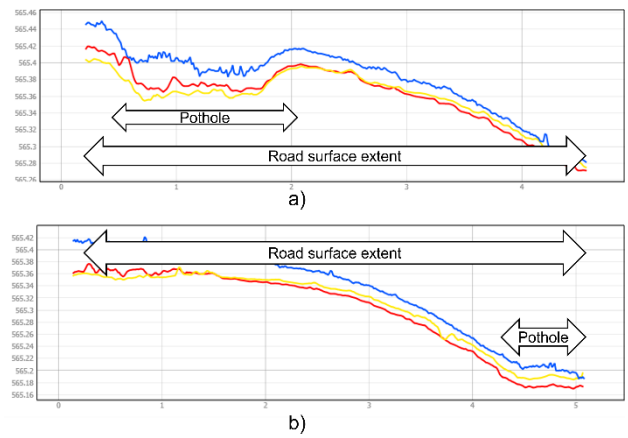

Figure 11. The largest (a) and smallest (b) road surface deformations of the study area, as seen on cross-views of the road surface; the *double_oblique* 3D model is represented in red, the *single_oblique* one in yellow and the *nadiral* one in blue. Note the transversal inclination of the road surface itself, with the right side approx. 0.25 cm lower than the left one.

3.3 Accuracy of volume estimation from close-range photogrammetric data

To establish the level of agreement between volumes determined from close-range photogrammetry and reference volumes determined by TLS, the difference between volumes was determined for each of the 32 defects and with statistical indicators for these errors were calculated (Table 2). Volumes from the *double_oblique* and *single_oblique* data collection approaches were also plotted against reference volumes (Figure 12).

Statistical indicator	Single_oblique data collection	Double_oblique data collection
Min. error (dm^3)	- 1.30	- 1.40
Max. error (dm^3)	2.80	2.50
Avg. error (dm^3)	0.28	0.28
Avg. unsigned error (dm^3)	0.66	0.67
Std. dev. (dm^3)	0.92	0.84
RMSE (dm^3)	0.18	0.16
Correl. coefficient R^2	.985	.991

Table 2: Agreement between road surface deformation volumes estimated from close-range photogrammetric data and laser scanning data collected by TLS.

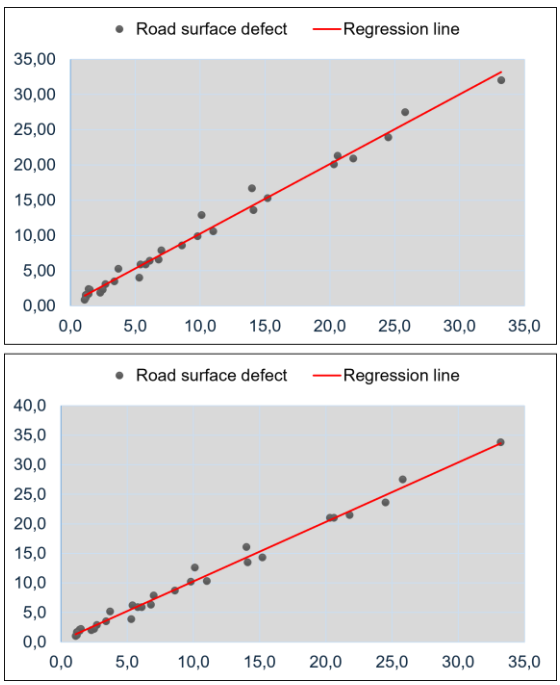

Figure 12. Correlation between defect volumes determined using close-range photogrammetric data collected using the *single_oblique* (top) and *double_oblique* (bottom) approach, and reference volumes determined from TLS data.

4. Conclusions

The aim of this study was to establish the potential of close-range photogrammetry (specifically, the SfM technique) for collecting data regarding the degradation of road surfaces, with the aid of a low-cost, widely available action camera (GoPro Hero 10). Images were collected over the study area, represented by a road sector of approx. 45 meters in length and affected by 32 road surface deformations (potholes). Three approaches were considered: *nadiral* (two parallel tracks following the road section, collected in a near-nadiral perspective from a height of approx. 2 meters), *single_oblique* (in which case the road surface was photographed a third time, in an inclined perspective) and

double_oblique (in which case a fourth set of images was collected, also in an inclined perspective but this time from the other side of the road). The road surface was also scanned using a Faro Focus S instrument, which is a professional, high-accuracy LiDAR equipment for scanning surfaces from fixed positions. The aim of this LiDAR scan was to serve as a reference, against which to compare 3D models of the road surface reconstructed from imagery collected using the GoPro action camera.

With the aid of GCPs accurately determined using a topographical survey (with total station + GNSS equipment) the models generated from overlapping images of the road surface can be scaled and georeferenced precisely, allowing for visual identification of defects and precise measurements of their characteristics, such as volume, area or depth. The use of GCPs also eliminates the risk of model drift, which is quite common for lengthy objects, even with more expensive camera setups. In terms of strategies for photogrammetric data collection, using only near-nadiral images lead to gaps in the 3D model near one side of the road, but this could potentially be alleviated by capturing images further from the object of interest (considering the inherent decrease in accuracy and resolution). Another potential approach, which was used in this study, is to complement the nadiral or near-nadiral images with oblique ones. This permitted a continuous 3D model of the road surface to be reconstructed, on which all defects could be identified and measured with ease.

Regarding the accuracy of volume estimations, we find that 3D models generated from images collected using a low-cost action camera accurately model all deformations, regardless of severity, with an average error of 0.28 cubic decimeters and R^2 values of 0.98-0.99.

Based on our analysis, we can highlight three main findings: (1) close-range photogrammetric data allows for a high-accuracy estimation of volumes for all road surface defects (regardless of severity), as compared to laser scanning carried out with a high-cost, high-performing LiDAR instrument, (2) adding oblique imagery allows for an even more accurate 3D reconstruction, with the average distance to the LIDAR point cloud improving from 0.013 to 0.007 meters and (3) adding a second band of oblique data collection (covering the road surface with oblique perspectives from both sides of it, i.e. the *double_oblique* approach) is not worth the additional labour, as it only adds a marginal increase of accuracy (RMSE of volume estimations improves by 12 percent when compared to the *single_oblique* approach, from 0.16 to 0.18 dm^3).

Overall, we consider that close-range photogrammetry is highly useful not only for obtaining 3D models of small objects, but also for reconstructing large areas, such as road sectors that are tens of meters in length, like the study area considered for this study. As such, this novel technique allows for monitoring road sectors, identifying road deformations and estimating their severity to a high degree of resolution and accuracy. In addition, these objectives are fulfilled at much lower costs when compared to established technologies (such as aerial/terrestrial laser scanning or using professional equipment designed specifically for monitoring road surfaces).

However, some limitations must be considered and could be the subject of further studies. The first one relates to GCPs and the potential of using metric bars to scale the models, thus eliminating the need for topographical surveys to determine GCP coordinates. The other main limitation is the amount of manual labour required to identify each deformation and calculate its volume, at least when using the approach described here. Therefore, developing an automatic method for detecting potholes (directly on points clouds or mesh models of the road surface) and for estimating their volumes is worthy of pursuit in future, planned studies.

References

Ahmed, M., Haas, C.T., Haas, R., 2011. Toward low-cost 3D automatic pavement distress surveying: the close range photogrammetry approach. *Can. J. Civ. Eng.* 38, 1301–1313. doi.org/10.1139/l11-088.

Akgul, M., Yurtseven, H., Akburak, S., Demir, M., Cigizoglu, H.K., Ozturk, T., Eksi, M., Akay, A.O., 2017. Short term monitoring of forest road pavement degradation using terrestrial laser scanning. *Measurement* 103, 283–293. doi.org/10.1016/j.measurement.2017.02.045.

Chen, Y.L., Jahanshahi, M.R., Manjunatha, P., Gan, W., Abdelbarr, M., Masri, S.F., Becerik-Gerber, B., Caffrey, J.P., 2016. Inexpensive Multimodal Sensor Fusion System for Autonomous Data Acquisition of Road Surface Conditions. *IEEE Sens. J. 16*, 7731–7743. doi.org/10.1109/JSEN.2016.2602871.

De Blasiis, M.R., Di Benedetto, A., Fiani, M., 2020. Mobile Laser Scanning Data for the Evaluation of Pavement Surface Distress. *Remote Sens.* 12, 942. doi.org/10.3390/rs12060942.

Del Pozo, S., Rodríguez-Gonzálvez, P., Hernández-López, D., Onrubia-Pintado, J., Guerrero-Sevilla, D., González-Aguilera, D., 2020. Novel Pole Photogrammetric System for Low-Cost Documentation of Archaeological Sites: The Case Study of "Cueva Pintada." *Remote Sens.* 12, 2644. doi.org/10.3390/rs12162644.

Dong, D., Li, Z., 2021. Smartphone Sensing of Road Surface Condition and Defect Detection. *Sensors* 21, 5433. doi.org/10.3390/s21165433.

Eker, R., 2023. Comparative use of PPK-integrated close-range terrestrial photogrammetry and a handheld mobile laser scanner in the measurement of forest road surface deformation. *Measurement* 206, 112322. doi.org/10.1016/j.measurement.2022.112322.

Gonçalves, J.A., Moutinho, O.F., Rodrigues, A.C., 2016. Pole photogrammetry with an action camera for fast and accurate surface mapping. *Int. Arch. Photogramm. Remote Sens. Spat. Inf. Sci.* XLI-B1, 571–575. doi.org/10.5194/isprs-archives-XLI-B1-571-2016.

Grygierek, M., Zieba, M., 2019. Damage to Road Pavements in the Area of Linear Discontinuous Deformations on the Surface Caused by Deep Mining. *IOP Conf. Ser. Earth Environ. Sci.* 362, 012151. doi.org/10.1088/1755-1315/362/1/012151.

Haiyan Guan, Li, J., Yongtao Yu, Chapman, M., Cheng Wang, 2015. Automated Road Information Extraction From Mobile Laser Scanning Data. *IEEE Trans. Intell. Transp. Syst.* 16, 194–205. doi.org/10.1109/TITS.2014.2328589.

Hrůza, P., Mikita, T., Tyagur, N., Krejza, Z., Cibulka, M., Procházková, A., Patočka, Z., 2018. Detecting Forest Road Wearing Course Damage Using Different Methods of Remote Sensing. *Remote Sens.* 10, 492. doi.org/10.3390/rs10040492.

James, M.R., Robson, S., 2012. Straightforward reconstruction of 3D surfaces and topography with a camera: Accuracy and geoscience application. *J. Geophys. Res. Earth Surf.* 117. doi.org/10.1029/2011JF002289.

Jia Yi, T., Ahmad, A.B., 2023. Quality Assessments of Unmanned Aerial Vehicle (UAV) and Terrestrial Laser Scanning (TLS) Methods in Road Cracks Mapping. Int. Arch. *Photogramm. Remote Sens. Spat. Inf. Sci.* XLVIII-4/W6-2022, 183–193. doi.org/10.5194/isprs-archives-XLVIII-4-W6-2022-183-2023.

Kargah-Ostadi, N., Nazef, A., Daleiden, J., Zhou, Y., 2017. Evaluation Framework for Automated Pavement Distress Identification and Quantification Applications. *Transp. Res. Rec. J. Transp. Res. Board* 2639, 46–54. doi.org/10.3141/2639-06.
Koch, C., Brilakis, I., 2011. Pothole detection in asphalt pavement images. *Adv Eng Inform.* 25, 507–515. doi.org/10.1016/j.aei.2011.01.002.

Kuželka, K., Surový, P., 2021. Mathematically optimized trajectory for terrestrial close-range photogrammetric 3D reconstruction of forest stands. *ISPRS J. Photogramm. Remote Sens.* 178, 259–281. doi.org/10.1016/j.isprsjprs.2021.06.013.

Lague, D., Brodu, N., Leroux, J., 2013. Accurate 3D comparison of complex topography with terrestrial laser scanner: Application to the Rangitikei canyon (N-Z). *ISPRS J. Photogramm. Remote Sens.* 82, 10–26. doi.org/10.1016/j.isprsjprs.2013.04.009.

Mokroš, M., Liang, X., Surový, P., Valent, P., Čerňava, J., Chudý, F., Tunák, D., Saloň, Š., Merganič, J., 2018. Evaluation of Close-Range Photogrammetry Image Collection Methods for Estimating Tree Diameters. *ISPRS Int. J. Geo-Inf.* 7, 93. doi.org/10.3390/ijgi7030093.

Morena, S., 2022. Application of action camera video for fast and low-cost photogrammetric survey of cultural heritage. *Int. Arch. Photogramm. Remote Sens. Spat. Inf. Sci.* XLVIII-2-W1-2022, 177–184. doi.org/10.5194/isprs-archives-XLVIII-2-W1-2022-177-2022.

Mroczkowski, K., 2009. Determining deformation on the road surface. *Rep. Geod.*, 277-281.

Nadal-Romero, E., Revuelto, J., Errea, P., López-Moreno, J.I., 2015. The application of terrestrial laser scanner and SfM photogrammetry in measuring erosion and deposition processes in two opposite slopes in a humid badlands area (central Spanish Pyrenees). Soil 1.2, 561–573. doi.org/10.5194/soil-1-561-2015.

Pankov, V., 2022. The problem of mechanical loads on pavement of roads in the cryolithic zone. *E3S Web Conf.* 363, 01039. doi.org/10.1051/e3sconf/202236301039.

Peraka, N.S.P., Biligiri, K.P., 2020. Pavement asset management systems and technologies: A review. *Autom. Constr.* 119, 103336. doi.org/10.1016/j.autcon.2020.103336.

Peter Heng, B.C., Chandler, J.H., Armstrong, A., 2010. Applying close range digital photogrammetry in soil erosion studies. *Photogramm. Rec.* 25, 240–265. doi.org/10.1111/j.1477-9730.2010.00584.x.

Pierzchała, M., Talbot, B., Astrup, R., 2016. Measuring wheel ruts with close-range photogrammetry. *For. Int. J. For. Res.* 89, 383–391. doi.org/10.1093/forestry/cpw009.

Pierzchała, M., Talbot, B., Astrup, R., 2014. Estimating Soil Displacement from Timber Extraction Trails in Steep Terrain: Application of an Unmanned Aircraft for 3D Modelling. *Forests* 5, 1212–1223. doi.org/10.3390/f5061212.

Sarsam, S.I., 2019. Comparative Assessment of Using Visual and Close Range Photogrammetry Techniques to Evaluate Rigid Pavement Surface Distresses. *Trends Transp. Engl. Appl.* 2, 28-36. doi:10.3759/ttea.v2i2.2814.

Sarsam, S.I., Daham, A.M., Ali, A.M., 2016. Assessing Close Range Photogrammetric Approach to Evaluate Pavement Surface Condition. *J. Eng.* 22, 1–14. doi.org/10.31026/j.eng.2016.01.01.

Smith, M.W., Vericat, D., 2015. From experimental plots to experimental landscapes: topography, erosion and deposition in sub-humid badlands from Structure-from-Motion photogrammetry. *Earth Surf. Process. Landf.* 40, 1656–1671. doi.org/10.1002/esp.3747.

Sun, C., Zhang, S., Xu, Z., Liu, A., Xu, S., Luo, Y., Li, J., 2023. Research on disaster evaluation of surface deformation in highway corridors based on MT-InSAR technology, in: *Second International Conference on Geographic Information and Remote Sensing Technology (GIRST 2023)*, SPIE, pp. 65–71. doi.org/10.1117/12.3007675.

Vilaça, J.L., Fonseca, J.C., Pinho, A.C.M., Freitas, E., 2010. 3D surface profile equipment for the characterization of the pavement texture – TexScan. *Mechatronics* 20, 674–685. doi.org/10.1016/j.mechatronics.2010.07.008.

Wang, H., Ji, L., Zhang, H., Lou, Y., Xu, L., Tan, Y., 2023. Indicator Construction of Road Surface Deformation Activity in Cold Regions and Its Relationship with the Distribution and Development of Longitudinal Cracks. *Sustainability* 15, 15466. doi.org/10.3390/su152115466.

Werkmeister, S., Canon Falla, G., Oeser, M., 2015. Analytical Design Methodology for Thin Surfaced Asphalt Pavements in Germany, in: *Airfield and Highway Pavements*, Miami, Florida, pp. 730–741. doi.org/10.1061/9780784479216.065.

Westoby, M.J., Brasington, J., Glasser, N.F., Hambrey, M.J., Reynolds, J.M., 2012. Structure-from-Motion photogrammetry: A low-cost, effective tool for geoscience applications. *Geomorphology* 179, 300–314. doi.org/10.1016/j.geomorph.2012.08.021.

Zeng, K.H., Guo, R.H., Li, H.X., 2013. Structural Response Analysis of Highways under Heavy Loads. *Adv. Mater. Res.* 723, 204–211. doi.org/10.4028/www.scientific.net/AMR.723.204.

Zhang, C., Elaksher, A., 2012. An Unmanned Aerial Vehicle-Based Imaging System for 3D Measurement of Unpaved Road Surface Distresses. *Comput.-Aided Civ. Infrastruct. Eng.* 27, 118–129. doi.org/10.1111/j.1467-8667.2011.00727.x.